Static Embedding with Pair Coupled Cluster Doubles Based Methods

Rahul Chakraborty, Katharina Boguslawski, and Paweł Tecmer

Institute of Physics, Faculty of Physics, Astronomy and Informatics,
Nicolaus Copernicus University in Torun,
Grudziadzka 5, 87-100 Torun, Poland

Supplementary Information

S1 XYZ Coordinates of $H_2O \cdots NH_3$ Complex

Table S1: XYZ Coordinates of the optimized $H_2O \cdots NH_3$ structure in Å.

N	-0.3247549	-1.0163481	0.2284577
H	0.3853716	-1.6985302	0.3923495
H	-0.9158405	-0.9874769	1.0326156
H	-0.8749286	-1.3247542	-0.5458969
O	0.3171256	1.9052994	-0.5156991
H	1.2106186	2.1227180	-0.3263054
H	0.2024080	0.9990920	-0.2655214

S2 EOM-CCSD vertical excitation energies of the H-bonded structures

TableS2: Vertical excitation energies (in eV) of $H_2O \cdots NH_3$ calculated with EOM-CCSD and aug-cc-pVDZ basis set. For each particular excitation, we show the VEE of the isolated source of excitation at the unrelaxed geometry of the complex.

Fragment		supramolecule
H_2O	NH_3	
	6.42	6.86
7.55		7.47
	7.96	8.43
	7.96	8.48

TableS3: The environmental shifts (ΔE_{env}) in vertical excitation energies (in eV) for the $H_2O \cdots NH_3$ complex calculated with EOM-pCCD-LCCSD and compared with EOM-CCSD values. ΔE_{env} is calculated as $(VEE_{\text{supra}} - VEE_{\text{frag}})$, where VEE_{supra} is the VEE of the supramolecule and VEE_{frag} is the same for the bare source of excitation at the unrelaxed geometry of the complex.

Source of excitation	EOM-pCCD-LCCSD	EOM-CCSD
NH_3	+0.43	+0.44
H_2O	-0.10	-0.08
NH_3	+0.46	+0.47
NH_3	+0.51	+0.52

Table S4: Vertical excitation energies (in eV) of thymine in micrsolvation calculated with EOM-CCSD and aug-cc-pVDZ basis set. ΔE_{env} is calculated as $(VEE_{\text{supra}} - VEE_{\text{frag}})$, where VEE_{supra} is the VEE of the supramolecule and VEE_{frag} is the same for the bare thymine at the unrelaxed geometry of the complex.

Thymine	Thymine in microsolvation	ΔE_{env}
5.34	5.86	+0.52
5.87	6.30	+0.43
6.77	7.15	+0.38

S3 Spin-Orbit Coupling

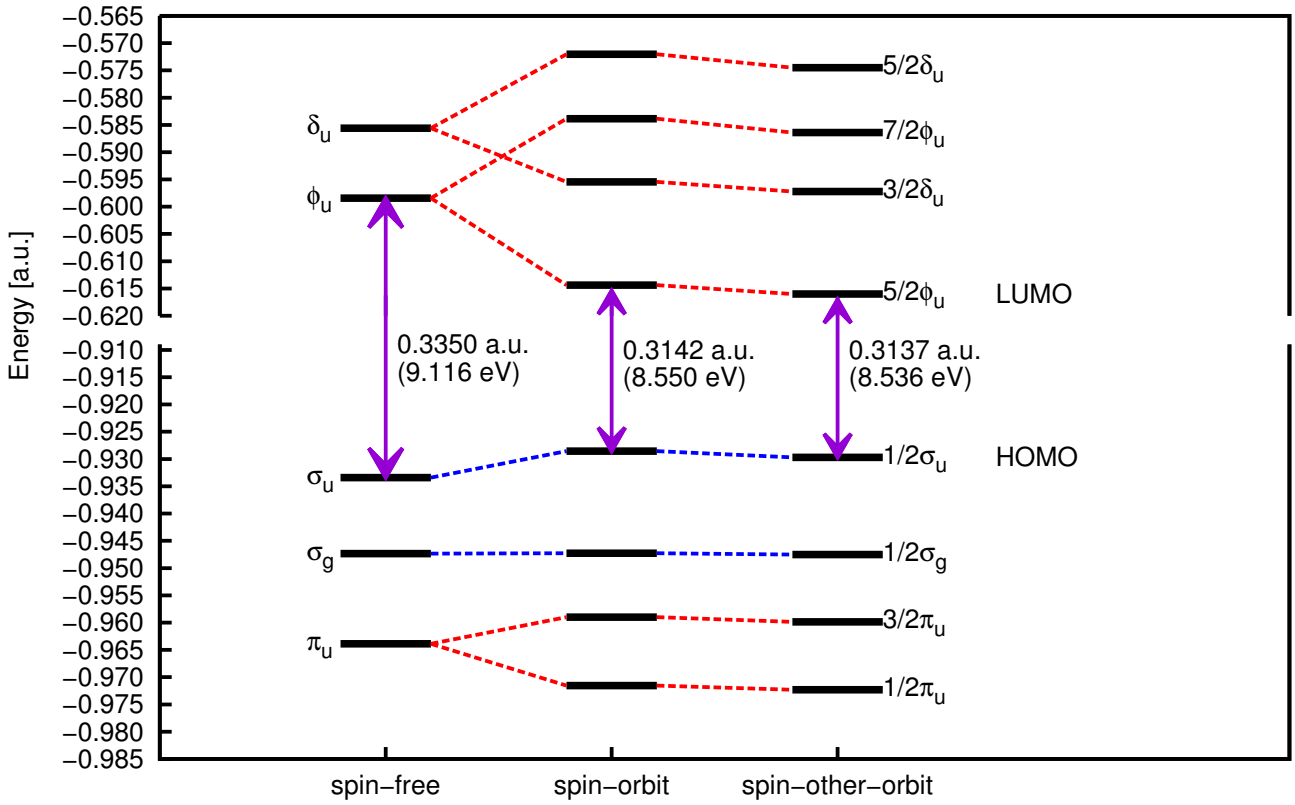

Figure S1: Comparison of Dirac–Hartree–Fock orbital energies of uranyl computed with different Hamiltonians: Dyall spin-free, (spin-orbit) Dirac–Coulomb, and Dirac–Coulomb–Breit (spin-other-orbit). The computations were performed with the Dirac2012 software package, aug-cc-pVTZ (O), and dyall.v3z (U) basis sets for U–O bond length of 1.708 Å.

S4 EOM-CCSD vertical excitation energies of uranyl tetrahalides

Table S5 shows the vertical excitation energies of the uranyl tetrahalides and the corresponding bare uranyl moieties. For the bare uranyl moieties, it is to be noted that the two δ_u orbitals are degenerate. We label them as δ_u and δ'_u to keep parity with the tetrahalides. We observe two transitions with both $\pi_u \rightarrow \delta_u$ and $\pi_u \rightarrow \delta'_u$ characters, in case of bare uranyls. For $UO_2Br_4^{2-}$, the $\pi_u \rightarrow \delta'_u$ transition is not observed with the 15 roots targeted in our EOM-CCSD calculation.

Table S5: EOM-CCSD/ANO-RCC-VDZP vertical excitation energies (in eV) of uranyl and its tetrahalides. The transitions are labelled according to their transition characters and not in the order of energies. The bare UO_2^{2+} calculations are done at each uranyl tetrahalide geometry, removing the halide atoms. The values in boldface in the 3rd column are the corresponding EOM-pCCD-LCCSD excitation energies of the bare uranyl, given here for comparison. Environmental shifts in EOM-CCSD excitation energies of uranyl due to the tetrahalide environment are given in the parenthesis in the 4th column.

System	Character (Term)	UO_2^{2+}	$UO_2X_4^{2-}$
$UO_2F_4^{2-}$	$\sigma_u \rightarrow \phi_u$ ($^1\Phi_g$)	3.02 **(3.50)**	4.22 (1.20)
	$\sigma_u \rightarrow \delta_u$ ($^1\Delta_g$)	3.39 **(3.89)**	3.89 (0.50)
	$\sigma_u \rightarrow \delta'_u$ ($^1\Delta_g$)	3.39 **(3.89)**	4.14 (0.75)
	$\pi_u \rightarrow \delta_u$ ($^1\Gamma_g$)	3.83 **(4.82)**	4.91 (1.08)
	$\pi_u \rightarrow \delta'_u$ ($^1\Pi_g$)	3.92 **(4.94)**	5.24 (1.32)
$UO_2Cl_4^{2-}$	$\sigma_u \rightarrow \phi_u$ ($^1\Phi_g$)	3.26 **(3.68)**	4.04 (0.78)
	$\sigma_u \rightarrow \delta_u$ ($^1\Delta_g$)	3.62 **(4.05)**	3.98 (0.36)
	$\sigma_u \rightarrow \delta'_u$ ($^1\Delta_g$)	3.62 **(4.05)**	4.08 (0.46)
	$\pi_u \rightarrow \delta_u$ ($^1\Gamma_g$)	4.16 **(5.02)**	5.01 (0.85)
	$\pi_u \rightarrow \delta'_u$ ($^1\Pi_g$)	4.25 **(5.13)**	5.08 (0.83)
$UO_2Br_4^{2-}$	$\sigma_u \rightarrow \phi_u$ ($^1\Phi_g$)	3.29 **(3.69)**	3.83 (0.54)
	$\sigma_u \rightarrow \delta_u$ ($^1\Delta_g$)	3.66 **(4.07)**	3.79 (0.13)
	$\sigma_u \rightarrow \delta'_u$ ($^1\Delta_g$)	3.66 **(4.07)**	3.87 (0.21)
	$\pi_u \rightarrow \delta_u$ ($^1\Gamma_g$)	4.21 **(5.05)**	4.44 (0.23)
	$\pi_u \rightarrow \delta'_u$ ($^1\Pi_g$)	4.30 **(5.16)**	–

S5 Orbital entropies and mutual information of uranyl tetrahalides

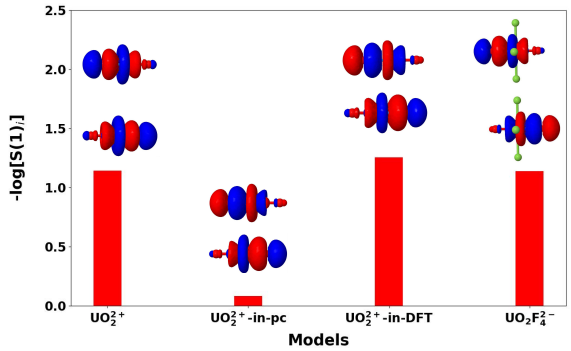

(**a**) σ_u

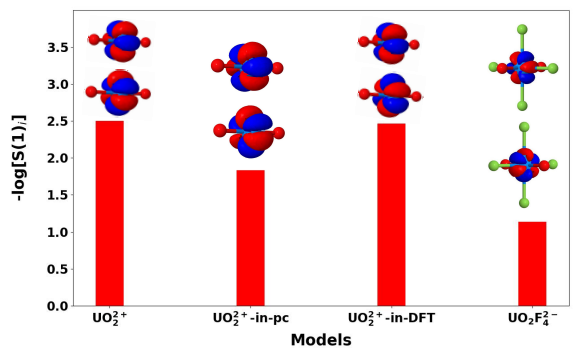

(**b**) ϕ_u

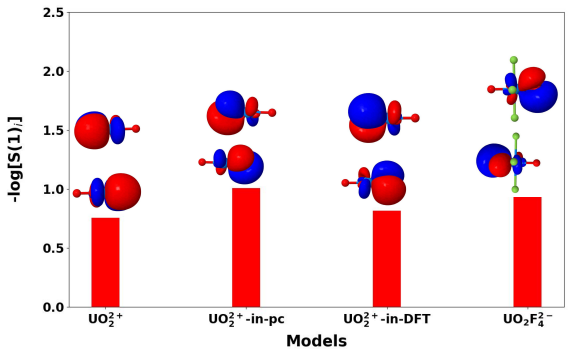

(**c**) π_u

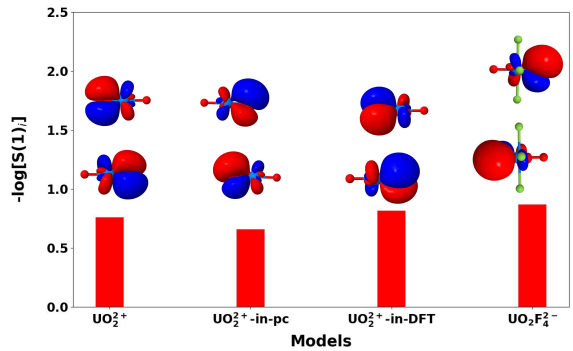

(**d**) π'_u

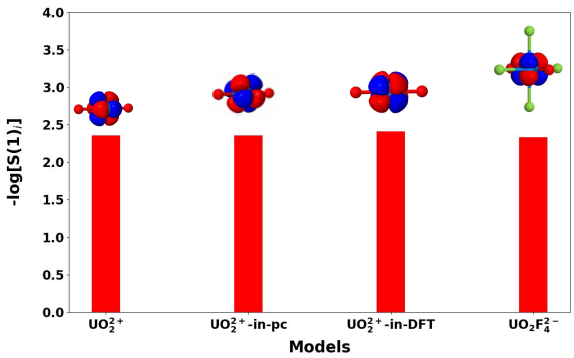

(**e**) δ_u

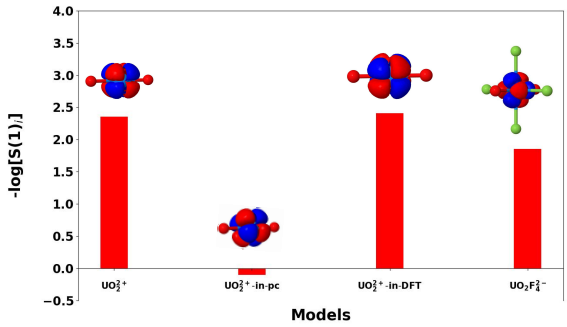

(**f**) δ'_u

Figure S2: Single-orbital entropies of $UO_2F_4^{2-}$ and related models.

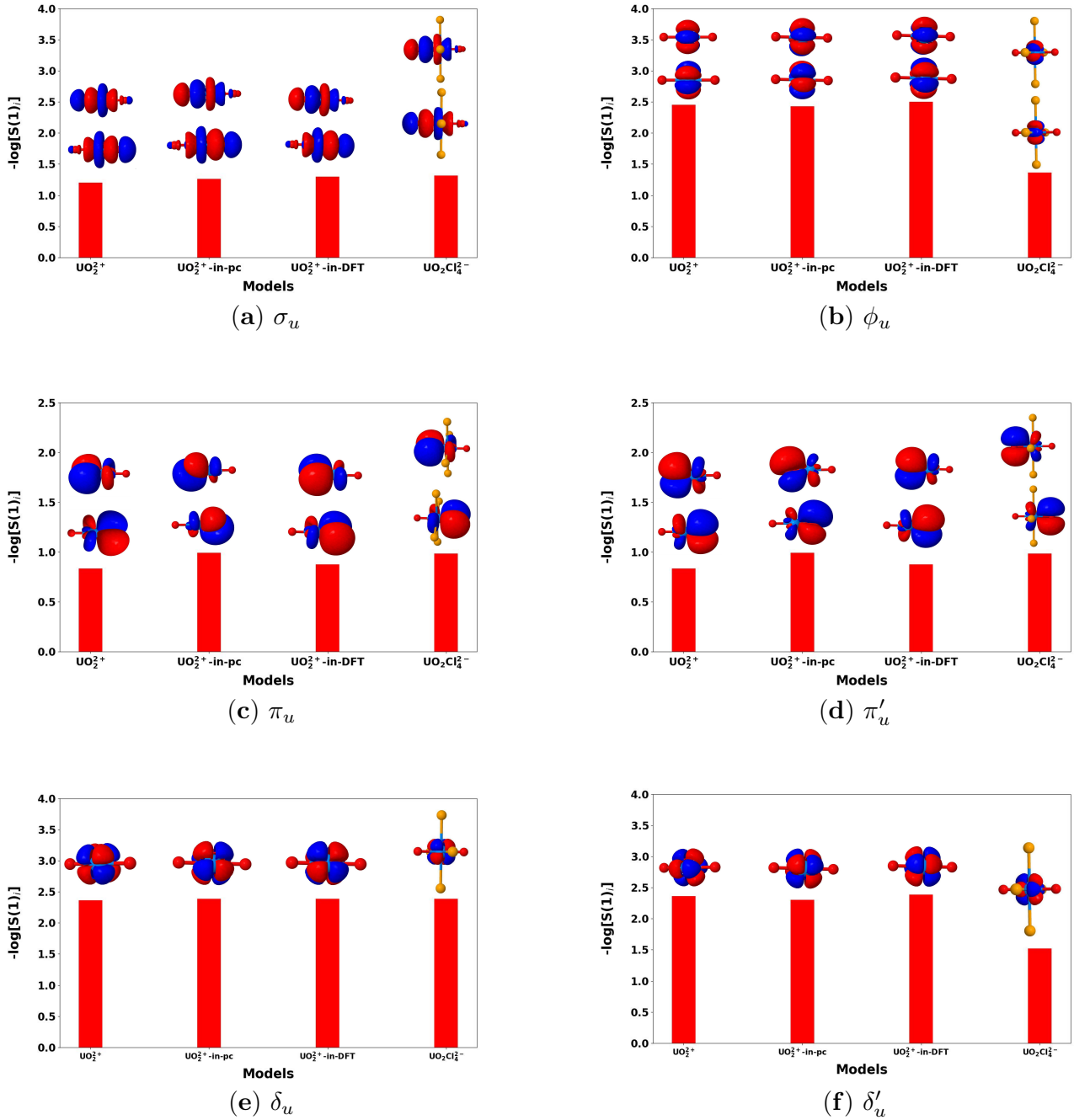

(**a**) σ_u (**b**) ϕ_u

(**c**) π_u (**d**) π'_u

(**e**) δ_u (**f**) δ'_u

Figure S3: Single-orbital entropies of $UO_2Cl_4^{2-}$ and related models.

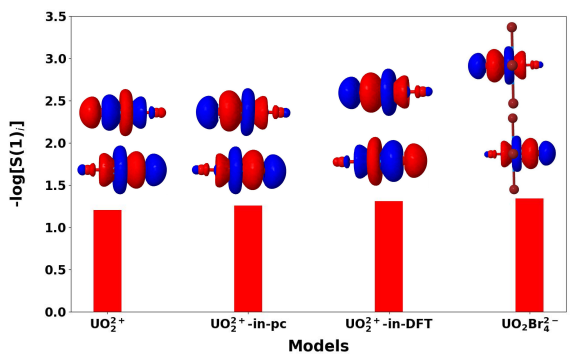

(**a**) σ_u

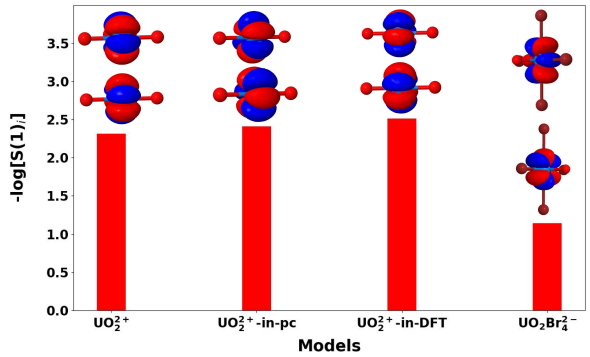

(**b**) ϕ_u

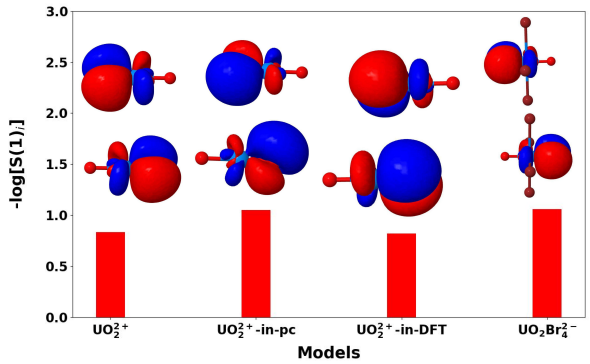

(**c**) π_u

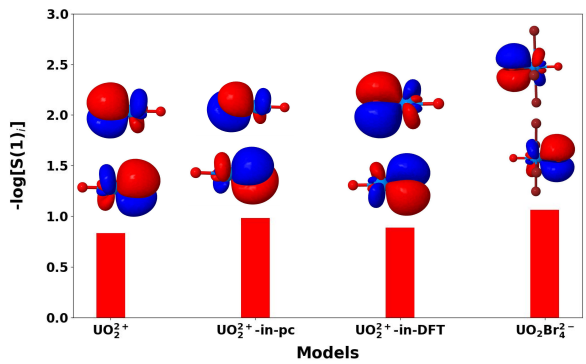

(**d**) π'_u

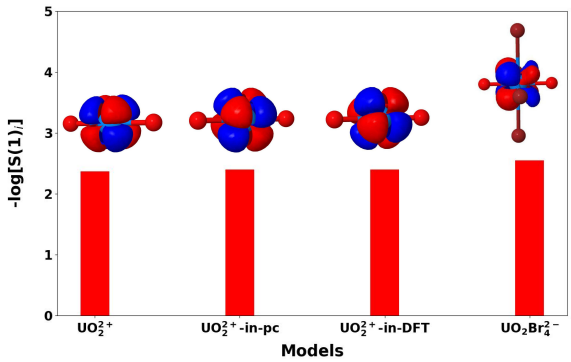

(**e**) δ_u

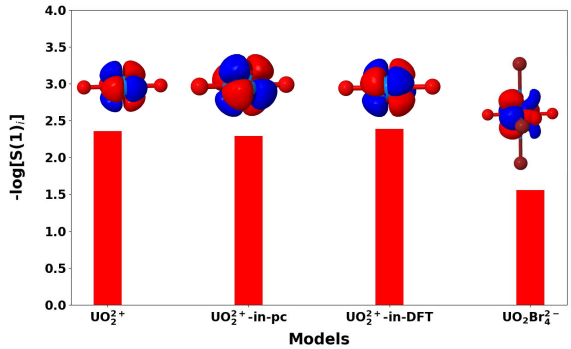

(**f**) δ'_u

Figure S4: Single-orbital entropies of $UO_2Br_4^{2-}$ and related models.

Table S6: Single-orbital entropies ($s(1)_i$) of the uranyl orbitals involved in the electronic spectra of the different moieties. The $s(1)_i$ values are calculated with the pCCD-LCCSD method.

System	Orbital	UO_2^{2+}	WFT-in-pc	WFT-in-DFT	Supramolecule
$UO_2F_4^{2-}$	σ_u	0.319	0.920	0.279	0.323
		0.319	0.921	0.292	0.324
	π_u	0.470	0.373	0.443	0.371
		0.470	0.359	0.443	0.402
		0.469	0.512	0.442	0.420
		0.469	0.526	0.442	0.421
	ϕ_u	0.082	0.087	0.085	0.209
		0.082	0.233	0.085	0.232
	δ_u	0.095	0.095	0.090	0.097
	δ'_u	0.095	1.11	0.090	0.157
$UO_2Cl_4^{2-}$	σ_u	0.292	0.281	0.273	0.266
		0.309	0.284	0.273	0.269
	π_u	0.434	0.362	0.417	0.373
		0.434	0.366	0.417	0.373
		0.434	0.370	0.417	0.373
		0.434	0.371	0.417	0.373
	ϕ_u	0.086	0.084	0.082	0.255
		0.086	0.092	0.082	0.255
	δ_u	0.094	0.092	0.092	0.092
	δ'_u	0.094	0.100	0.092	0.219
$UO_2Br_4^{2-}$	σ_u	0.300	0.279	0.269	0.260
		0.300	0.290	0.270	0.264
	π_u	0.435	0.344	0.411	0.346
		0.435	0.354	0.411	0.346
		0.435	0.372	0.411	0.345
		0.435	0.375	0.411	0.345
	ϕ_u	0.099	0.090	0.081	0.319
		0.099	0.090	0.081	0.320
	δ_u	0.094	0.091	0.091	0.078
	δ'_u	0.095	0.101	0.092	0.211

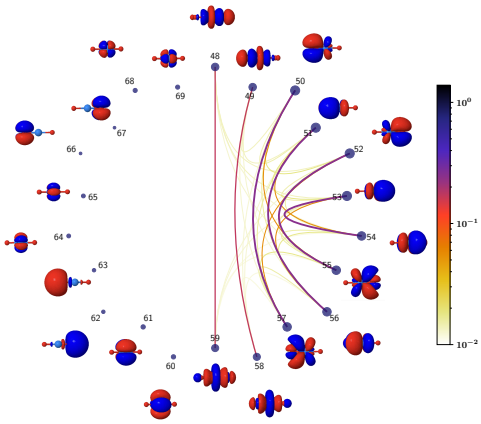

(**a**) UO_2^{2+}

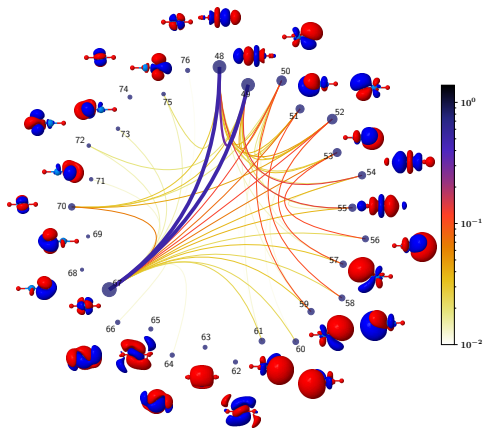

(**b**) UO_2^{2+}-in-pc

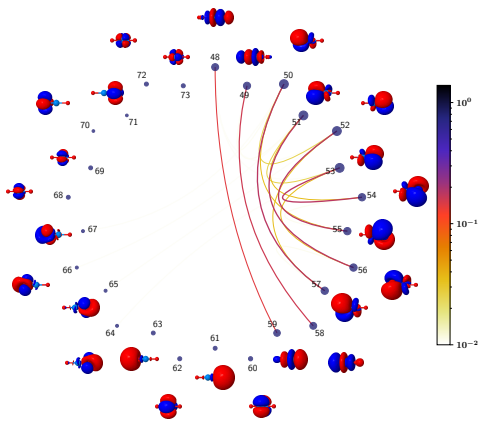

(**c**) UO_2^{2+}-in-DFT

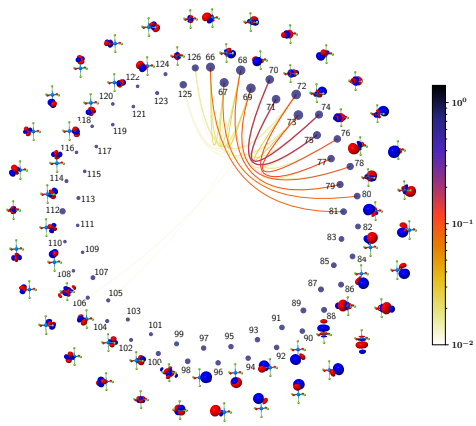

(**d**) $UO_2F_4^{2-}$

Figure S5: Mutual information ($I_{i|j}$) of $UO_2F_4^{2-}$ and related models studied in this work. The orbitals are numbered as obtained after pCCD optimization. The $I_{i|j}$ values are calculated based on single-orbital entropies calculated with the pCCD-LCCSD method.

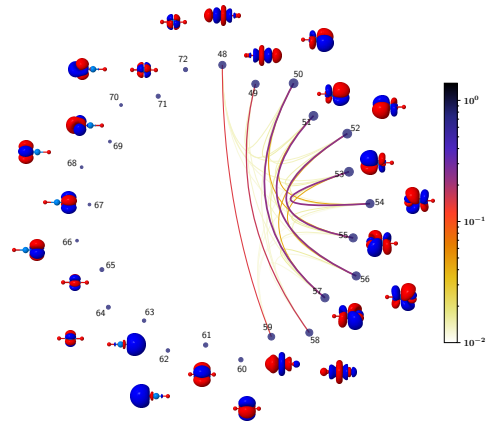

(**a**) UO_2^{2+}

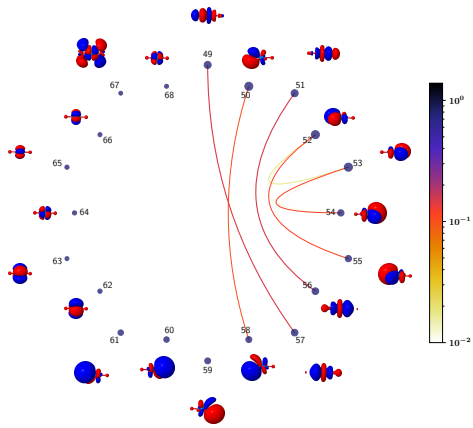

(**b**) UO_2^{2+}-in-pc

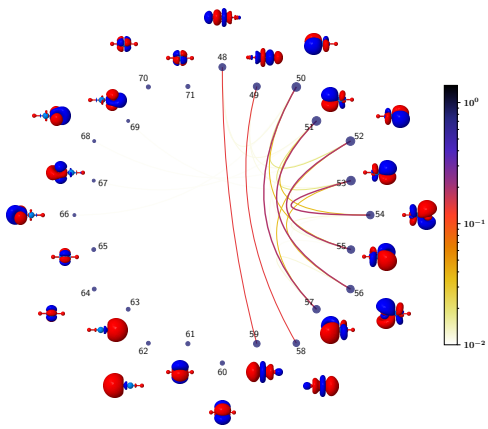

(**c**) UO_2^{2+}-in-DFT

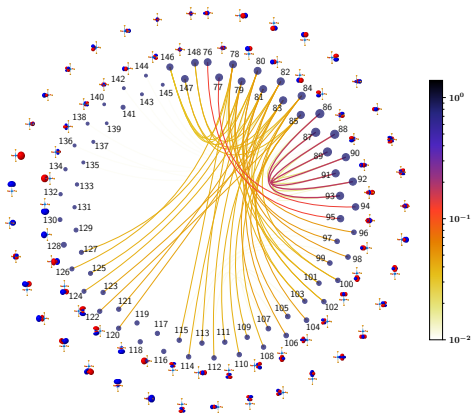

(**d**) $UO_2Cl_4^{2-}$

Figure S6: Mutual information ($I_{i|j}$) of $UO_2Cl_4^{2-}$ and related models studied in this work. The orbitals are numbered as obtained after pCCD optimization. The $I_{i|j}$ values are calculated based on single-orbital entropies calculated with the pCCD-LCCSD method.

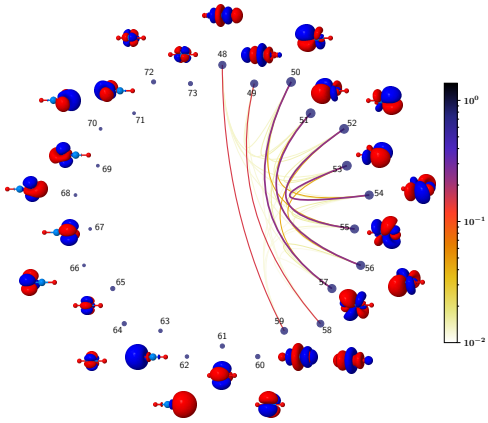

(**a**) UO_2^{2+}

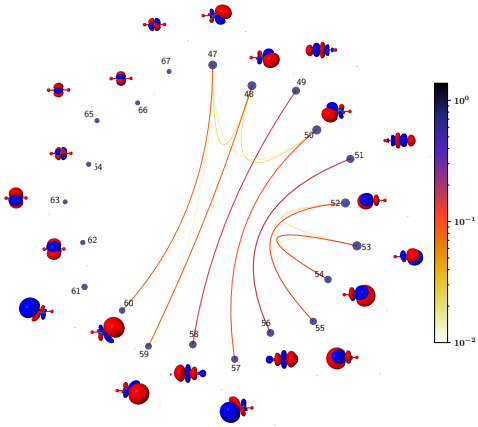

(**b**) UO_2^{2+}-in-pc

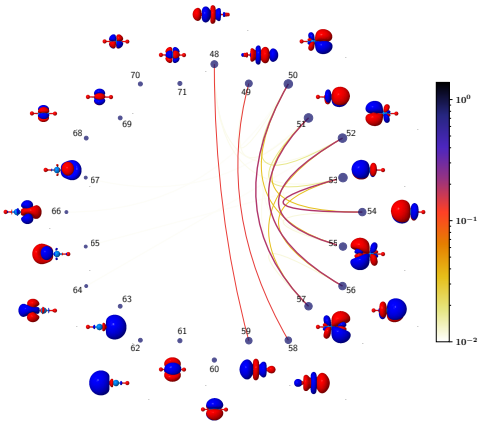

(**c**) UO_2^{2+}-in-DFT

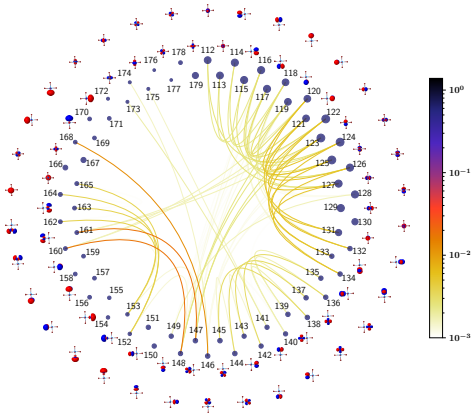

(**d**) $UO_2Br_4^{2-}$

Figure S7: Mutual information ($I_{i|j}$) of $UO_2Br_4^{2-}$ and related models studied in this work. The orbitals are numbered as obtained after pCCD optimization. The $I_{i|j}$ values are calculated based on single-orbital entropies calculated with the pCCD-LCCSD method.